

# Greater variability in local vegetation structure increases forest resistance to wildfire

MICHAEL J KOONTZ<sup>1</sup>, MALCOLM P NORTH<sup>1, 2</sup>, STEPHEN E FICK<sup>3</sup>, CHHAYA M WERNER<sup>4</sup>, and ANDREW M LATIMER<sup>1</sup>

<sup>1</sup>*Graduate Group in Ecology, University of California, Davis, CA 95616 USA*

<sup>2</sup>*USDA Forest Service, Pacific Southwest Research Station, Davis, CA 95618 USA*

<sup>4</sup>*Stockholm Environment Institute, Stockholm 115 23, Sweden*

<sup>5</sup>*Center for Population Biology, University of California, Davis, CA 95616 USA*

**Abstract.** Variation in the size and distribution of trees can enable a forest to withstand ongoing disturbances and retain its essential identity and function. We test this phenomenon at a broad spatial extent in California's Sierra Nevada region using remotely-sensed data corroborated with on the ground measurements. We find that greater heterogeneity in local forest structure reduces the severity of wildfires. Heterogeneous forest structure thus makes mixed conifer forest in the Sierra Nevada more resistant to this inevitable disturbance, and may increase the probability of its long-term persistence. Management activities that seek to increase forest heterogeneity, such as prescribed fire, should be continued.

*Key words:* resilience; wildfire severity; RdNBR; remote sensing

## INTRODUCTION

Three intertwining themes:

1. Resilience of disturbance-prone (e.g., wildfire) systems is important basic ecological question with dramatic socio-ecological consequences. We can measure part of resilience by recognizing panarchy and measuring how heterogeneous vegetation promotes forest resistance at very broad scales.
2. We can measure severity in a programmatic way to get comparable data across broader spatial and deeper temporal extents.
3. We can apply texture analysis to vegetation to quantify heterogeneity.

Biological systems comprising heterogeneous elements can retain their fundamental properties in the face of regular disturbance. This ability of a heterogeneous system to absorb disturbances, reorganize, and to persist within a domain of stability with respect to its identity, structure, function, and feedbacks is termed resilience (Holling 1973; Gunderson 2000; Folke *et al.* 2004; Walker *et al.* 2004). Resilience (*sensu* Walker *et al.* (2004)) is characterized by four critical features: 1) latitude, which describes the degree to which a system can deviate from an attracting state and still recover to that state, 2) resistance, which describes the intensity or duration of a disturbance required to change the system state, 3) precariousness, which describes the proximity of a system to a threshold of a different domain of stability, and 4) panarchy, which describes how resilience features interact across multiple scales of organization. Resilience has been demonstrated in complex biological systems characterized by a variety of different types of "heterogeneity" including genetic diversity (Reusch *et al.* 2005; Agashe 2009; Baskett *et al.* 2009), species diversity (Tilman 1994; Chesson 2000;

Cadotte *et al.* 2013), functional diversity (Gazol & Camarero 2016), topoclimatic complexity (Ackerly *et al.* 2010, @Lenoir2013), and temporal environmental variation (Questad & Foster 2008). An emerging paradigm in forest ecology is that spatial heterogeneity in the structure of vegetation on the landscape can confer resilience to disturbances such as wildfire, drought, and insect outbreaks (Stephens *et al.* 2008; North *et al.* 2009; Virah-Sawmy *et al.* 2009). Forests are globally important ecosystems threatened in a number of ways, and protection of forests is of high management priority (Hansen *et al.* 2013; Crowther *et al.* 2015; Millar & Stephenson 2015; Trumbore *et al.* 2015). Thus, it is critical to understand the mechanisms underlying the effect of spatial heterogeneity in forest structure on forest resilience.

Forest structure is defined by the size and distribution of trees on the landscape. Differences in tree crown heights characterize vertical structure, while differences in the rooting locations of trees characterizes horizontal structure (North *et al.* 2009). Structural patterns can be further parsed by the constituent species present. In the Sierra Nevada range of California, forests are dominated by a mixture of conifer species including ponderosa pine (*Pinus ponderosa*), sugar pine (*Pinus lambertiana*), incense-cedar (*Calocedrus decurrens*), Douglas-fir (*Pseudotsuga menziesii*), white fir (*Abies concolor*), and red fir (*Abies magnifica*) (Stephens & Collins 2004; Collins *et al.* 2015). Tree density in the early 20th century was relatively low, with about 25-79 trees/ha and about 8-30 m<sup>2</sup>/ha of live basal area (Collins *et al.* 2015). Previous work described the historical distribution of trees in the Sierra Nevada as an “ICO pattern,” which refers to its three distinct features: individual trees (I), clumps of trees with interlocking crowns (C), and openings with no tree cover at all (O) (Larson & Churchill 2012). The ICO pattern manifests at small spatial extents between 0.2 and 1.2 ha and is maintained by feedbacks with spatially explicit ecological processes (Larson & Churchill 2012; Lydersen *et al.* 2013; Fry *et al.* 2014). Competition for light, water, and other resources can yield aggregations of trees within favorable microsites or more widely spaced trees to ameliorate detrimental interactions (Clyatt *et al.* 2016). Demographic processes of dispersal, recruitment, and mortality affect forest structure by adding or subtracting whole trees. Reciprocally, the forest structure can also influence these pattern-forming processes such as when vegetation overstory alters microclimate or changes tree demographic rates (Larson & Churchill 2012; De Frenne *et al.* 2013; Ford *et al.* 2013). The stabilizing effects of these reciprocal processes in forests are hallmarks of a resilient system (Folke *et al.* 2004). In the Sierra Nevada range of California, the strongest feedbacks between forest structure and pattern-generating ecological process relate to the widespread disturbances caused by wildfire and bark beetle outbreaks (Raffa *et al.* 2008; Larson & Churchill 2012; Millar & Stephenson 2015). Wildfire and bark beetle outbreaks both kill live trees, affect hundreds of thousands to millions of hectares of forested area per year, and interact dynamically with the forest structures they encounter (Westerling *et al.* 2006; Raffa *et al.* 2008; Larson & Churchill 2012; Park Williams *et al.*

2012).

In an ecological framework, wildfire is typically classified into different fire regimes that describe how frequently and how intensely they burn (Keeley *et al.* 2011; Mandle *et al.* 2011; Steel *et al.* 2015). For instance, mixed conifer forests in the Sierra Nevada burned every 11 years on average for several centuries prior to Euro-American settlement (Steel *et al.* 2015). These relatively frequent burns prevented the accumulation of fuel on the ground, and limited the intensity of the next fire. This average fire return interval is short compared to the regeneration time of the dominant species, so the fire regime of Sierra Nevada mixed conifer forests in this period is usually classified as a “high frequency/low-mid severity” (Steel *et al.* 2015). However, wildfire behavior is inherently complex and is influenced by local weather, topography, and heterogeneous fuel conditions created by departures from the average fire return interval at any particular place (Sugihara & Barbour 2006; Collins & Stephens 2010). Wildfire can affect the future forest structure by changing demographic rates of individual trees (e.g. increasing growth or germination via increasing light or nitrogen availability), but its most lasting impact to forest structure is in the pattern of killed trees left in its wake (Larson & Churchill 2012). Reciprocally, forest structure can influence fire behavior: for instance, high tree density and presence of “ladder fuels” in the understory increase the probability of crown fire that kills a high proportion of trees (Stephens *et al.* 2008; North *et al.* 2009).

Severity describes the effect of a wildfire on an ecosystem— often the amount of vegetation mortality (Sugihara & Barbour 2006). Wildfire severity can be measured by comparing pre- and post-fire satellite imagery for a specific area, but this usually requires considerable manual effort for image collation and processing, followed by calibration with field data (Miller & Thode 2007; Miller *et al.* 2009; De Santis *et al.* 2010; Cansler & McKenzie 2012; Veraverbeke & Hook 2013; Parks *et al.* 2014; Prichard & Kennedy 2014; Edwards *et al.* 2018; Fernández-García *et al.* 2018). Efforts to measure severity across broad spatial extents, such as the Monitoring Trends in Burn Severity project (Eidenshink *et al.* 2007), are unsuitably subjective for rigorous scientific analysis though they serve their intended management purpose admirably (Kolden *et al.* 2015). Automated efforts to remotely assess wildfire have arisen, but they tend to focus on more aggregate measures of wildfire such as whether an area burned or the probability that it burned rather than the severity of the burn (Bastarrika *et al.* 2011; Goodwin & Collett 2014; Boschetti *et al.* 2015; Hawbaker *et al.* 2017). Here, we present a method to automate the measurement of wildfire severity using minimal user inputs: a geometry of interest (a wildfire perimeter or a field plot location) and an alarm date (the date the fire began). This information is readily available in many fire-prone areas (such as California, via the Fire and Resource Assessment Program; [http://frap.fire.ca.gov/projects/fire\\_data/fire\\_perimeters\\_index](http://frap.fire.ca.gov/projects/fire_data/fire_perimeters_index)) or could potentially be derived using existing products (such as the Landsat Burned Area Essential Climate Variable

product described in Hawbaker *et al.* (2017)). Further, the flexibility of this approach facilitates collaborative calibration with field-collected wildfire severity data.

Vegetation characteristics such as canopy density (Rouse *et al.* 1973; Young *et al.* 2017), moisture content (Asner *et al.* 2015), insect attack (Näsi *et al.* 2015), and even functional diversity (Asner *et al.* 2017) can be measured using remotely-sensed imagery. Texture analysis of imagery can quantify ecologically relevant environmental heterogeneity across broad spatial scales (Wood *et al.* 2012). Texture analysis was originally developed for image classification and computer vision, and it characterizes each pixel in an image by a summary of its neighboring pixels (Haralick *et al.* 1973; Connors *et al.* 1984). Ecologists have successfully used texture to augment predictions of species richness (Huang *et al.* (2014); Stein *et al.* (2014); Tuanmu & Jetz (2015) but see Culbert *et al.* (2012)).

Resilience has gained new attention in light of anthropogenic global change because of the potential for novel disturbance regimes to exceed a system’s capacity to recover (Millar *et al.* 2007; Turner *et al.* 2013). Beyond these thresholds, catastrophic shifts in ecosystems are likely, with myriad consequences for ecosystems and the services they provide (Scheffer *et al.* 2001; Turner *et al.* 2013). Changes in wildfire disturbance regimes are particularly suited to catalyze catastrophic shifts in ecosystems because of their feedback with spatial forest heterogeneity at multiple scales. Anthropogenic global change and a century of fire suppression policy in the United States have resulted in forest conditions far outside their range of historic variability, with potentially dire consequences for society (North *et al.* 2015). In California, increasing temperature couples with increasing drought frequency to exacerbate water stress and drive tree mortality during “hotter droughts” (Park Williams *et al.* 2012; Millar & Stephenson 2015). Further, a century of fire suppression policy has led to drastic changes in forest structure (North *et al.* 2015). Canopy cover has increased by 25-49%, overall tree density has increased by >75%, and white fir (*Abies concolor*) makes up a greater percentage of basal area compared to forests in the early 20th century (Stephens *et al.* 2015). The change in tree density is underlain by a shift in size distribution: modern mixed conifer forests have 2.5 times as many trees between 30.4 and 61.0cm diameter at breast height (dbh) per hectare (103.9 versus 41.0 trees/ha) and half as many trees greater than 91.4cm dbh per hectare (8.7 versus 16.7 trees/ha) compared to forests in 1911 (Stephens *et al.* 2015). Thus, western North American forests are experiencing novel, “unhealthy” conditions (*sensu* Raffa *et al.* (2009)) that are liable to upset the feedbacks between forest structure and pattern-forming ecological disturbances that historically stabilized the system and made it resilient (Raffa *et al.* 2008; Millar & Stephenson 2015).

A forest that is resistant to wildfire will be less impacted following a disturbance of that type. In forests with relatively intact fire regimes and heterogeneous stand conditions such as in the Jeffrey pine forests of the

Sierra San Pedro Martir in Baja, California, there tends to be reduced vegetation mortality after wildfires compared to fire-suppressed forests (Stephens *et al.* 2008). A heterogeneous forest can largely avoid overstory tree mortality because a reduced amount of accumulated ladder fuel decreases its ability to get into the crown (where mortality is more likely to result), because widely-spaced tree clumps interrupt fire spread across the landscape, and because tree clumps with fewer trees don't facilitate self-propagating fire behavior (Graham *et al.* 2004; Scholl & Taylor 2010). Thus, forests with heterogeneous structure are predicted to persist in that state due to resistance to inevitable wildfire disturbance (Graham *et al.* 2004; Moritz *et al.* 2005; Stephens *et al.* 2008). However, it is unclear whether this is true at broad spatial extents, nor is it resolved at what scale heterogeneity in forest structure is meaningful for resilience (Kotliar & Wiens 1990).

Does spatial variability in forest structure confer resilience to California mixed conifer forests by reducing the severity of wildfires when they occur?

## Methods

This work occurred in two phases. First, we developed a new approach to calculating wildfire severity across broad spatial and temporal scales and calibrated our measurements to those from the field. We applied this approach to all known fire perimeters in the Sierra Nevada region between 1984 and 2016 as defined by the Fire and Resource Assessment Program (FRAP, [http://frap.fire.ca.gov/projects/fire\\_data/fire\\_perimeters\\_index](http://frap.fire.ca.gov/projects/fire_data/fire_perimeters_index)), which is the most comprehensive digital record of fire occurrence in California. Second, we used texture analysis of remotely-sensed imagery bounded by the perimeters in the FRAP database to develop a measure of vegetation heterogeneity and modeled how that heterogeneity affected wildfire severity, accounting for other key drivers of wildfire behavior. ## A new approach to remotely sensing wildfire severity

The Thematic Mapper (TM; Landsat 4 and 5), Enhanced Thematic Mapper Plus (ETM+; Landsat 7), and Operational Land Imager (OLI; Landsat 8) sensors generate compatible top-of-atmosphere (TOA) spectral reflectance data suitable for scientific analysis. Recent advances in radiometric correction post-processing can compensate for various atmospheric distortions and generate more accurate measurements of surface reflectance in narrow wavelength bands spanning the electromagnetic spectrum (Masek *et al.* 2006; Vermote *et al.* 2016; USGS 2017b, a). Landsat satellites image the entire Earth approximately every 16-days and repeat images of the same area are geometrically coregistered such that overlapping pixels correspond to the same area on the ground. We used Google Earth Engine, a cloud-based geographic information system and image hosting platform, for all image collation and processing in order to leverage the centralized availability of the latest processed satellite images and integrated image processing tools for broad-scale analyses (Gorelick

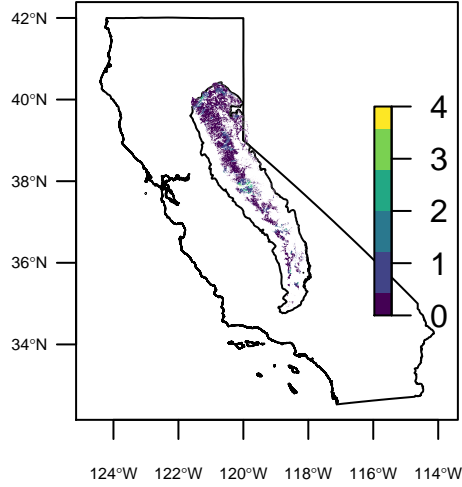


Figure 1: Locations of fires in yellow pine/mixed conifer forests in the Sierra Nevada mountain range of California. Colored pixels are designated yellow pine/mixed conifer according to the presettlement fire regime from the FRID database. Colors represent the number of fires that burned in that area during the satellite era.

*et al.* 2017).

## Collation of pre- and post-fire imagery

We collated and processed Landsat imagery

Individual Landsat images (a.k.a. “scenes”) represent an area on the Earth’s surface approximately 170 km long by 183 km wide.

## Wildfire severity

The normalized difference vegetation index (NDVI) can be used to assess canopy density, and it was calculated for all pixels using the near infrared band and the red band (Rouse *et al.* 1973):

$$NDVI = \frac{NIR - RED}{NIR + RED} \quad (1)$$

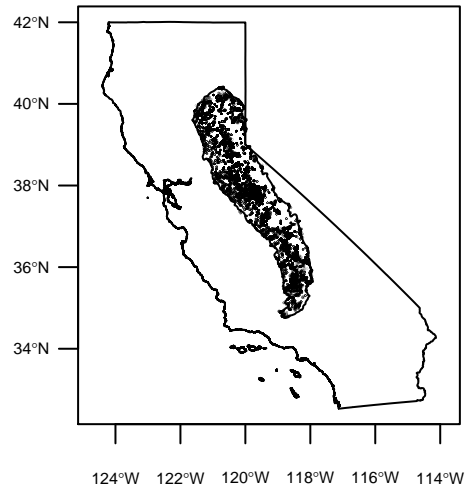


Figure 2: Locations of samples from fires in yellow pine/mixed conifer forests in the Sierra Nevada mountain range of California.

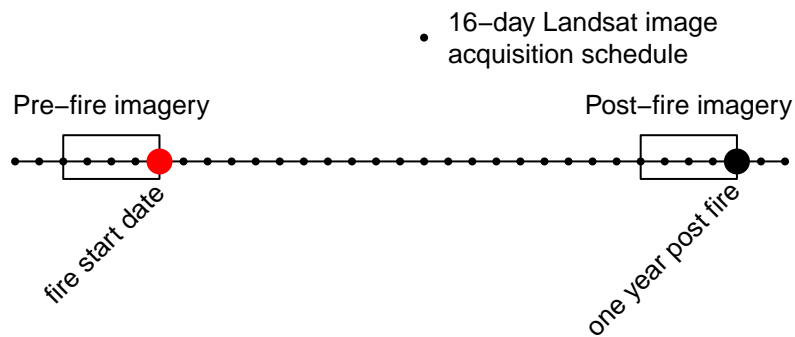


Figure 3: Schematic for how Landsat imagery was assembled in order to make comparisons between pre- and post-fire conditions. This schematic depicts a 64-day window of image collation prior to the fire which comprise the pre-fire image collection. A similar, 2-month window collection of imagery is assembled one year after the pre-fire image collection.

Where NIR is the near infrared band (band 4 on Landsat 4, 5, and 7; band 5 on Landsat 8) and RED is the red band (band 3 on Landsat 4, 5, and 7; band 4 on Landsat 8).

The normalized difference moisture index (NDMI) can be used to assess canopy density, and it was calculated for all pixels using the near infrared band and the red band (Gao 1996):

$$NDMN = \frac{NIR - SWIR1}{NIR + SWIR1} \quad (2)$$

Where NIR is the near infrared band (band 4 on Landsat 4, 5, and 7; band 5 on Landsat 8) and SWIR1 is the first short wave infrared band (band 5 on Landsat 4, 5, and 7; band 4 on Landsat 8).

The normalized burn ratio is calculated as (Key & Benson 2006; USGS 2017a, b)

$$NBR = \frac{NIR - SWIR2}{NIR + SWIR2} \quad (3)$$

Where NIR is the near infrared band (band 4 on Landsat 4, 5, and 7; band 5 on Landsat 8) and SWIR2 is the second short wave infrared band (band 7 on Landsat 4, 5, 7, and 8)

The normalized burn ratio version 2 (NBR2) is calculated as (Hawbaker *et al.* 2017; USGS 2017a, b):

$$NBR2 = \frac{SWIR1 - SWIR2}{SWIR1 + SWIR2} \quad (4)$$

Where SWIR1 is the first short wave infrared band (band 5 on Landsat 4, 5, and 7; band 6 on Landsat 8) and SWIR2 is the short wave infrared band (band 7 on Landsat 4, 5, 7, and 8).

### Calculation of wildfire severity

Wildfire severity can be reliably detected remotely by comparing pre- and post-fire imagery from the Landsat series of satellites (Eidenshink *et al.* 2007; Miller & Thode 2007). We calculated remotely-sensed wildfire severity using the relative burn ratio (RBR) (Parks *et al.* 2014), the delta normalized burn ratio (dNBR) (Eidenshink *et al.* 2007; Miller & Thode 2007), the relative differenced normalized burn ratio (RdNBR) (Miller & Thode 2007), the delta normalized burn ratio 2 (dNBR2) (Hawbaker *et al.* 2017), and the relative differenced normalized burn ratio 2 (RdNBR2). For all remotely-sensed severity metrics, we did not calculate the “offset” per fire, which



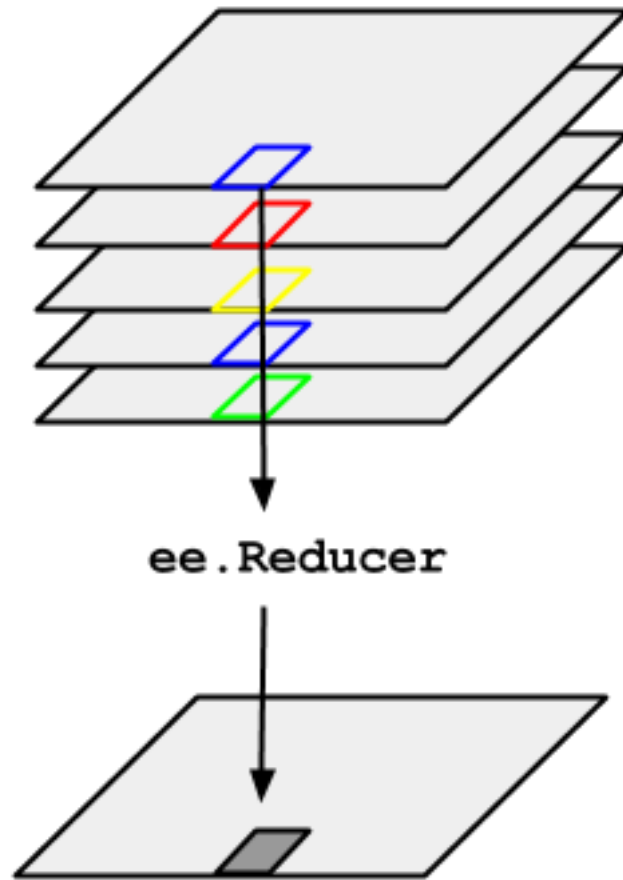


Figure 4: Reductions of an image collection that characterize each pixel as a summary statistic of a stack of corresponding pixels at different points in time. In our case we summarize a time series of each pixel into the median value across that series. Image courtesy of Google and can be found at [https://developers.google.com/earth-engine/reducers\\_image\\_collection](https://developers.google.com/earth-engine/reducers_image_collection)

189 We calculated the differenced versions of these indices by subtracting the post-fire index from the pre-fire  
 190 index without multiplying by a rescaling constant (e.g., we did not multiply the result by 1000 as in Miller &  
 191 Thode (2007)):

$$dINDEX = INDEX_{\text{prefire}} - INDEX_{\text{postfire}} \quad (5)$$

$$RBR = \frac{dNBR}{NBR_{\text{prefire}} + 1.001} \quad (6)$$

192 Prefire values of these indices are calculated by first calculating them for each image in the prefire image  
 193 collection, and then using a median reducer across the stack of images (see Fig. 4).

$$RdINDEX = \frac{dINDEX}{\sqrt{|INDEX_{\text{prefire}}|}} \quad (7)$$

#### 194 **Calibrating remotely-sensed wildfire severity with field-measured wildfire severity**

195 We calibrated our remotely-sensed measure of wildfire severity with 208 field measures of overstory tree  
 196 mortality from two previously published studies (Zhu *et al.* 2006; Sikkink *et al.* 2013) (Fig. 5). The  
 197 Composite Burn Index (CBI) is a metric of change in vegetation across several vertical strata (Key & Benson  
 198 2006) and has a long history of use in calibrating remotely-sensed severity data (Miller & Thode 2007; Miller  
 199 *et al.* 2009; Cansler & McKenzie 2012; Parks *et al.* 2014; Prichard & Kennedy 2014). Following Miller &  
 200 Thode (2007), Miller *et al.* (2009), and Parks *et al.* (2014), we fit a non-linear model to each remotely-sensed  
 201 severity metric of the following form:

$$\text{remote\_severity} = \beta_0 + \beta_1 e^{\beta_2 \text{cbi\_overstory}} \quad (8)$$

202 We fit the model in Eq. 8 for all 7 of our remotely-sensed severity metrics (RBR, dNBR, RdNBR, dNBR2,  
 203 RdNBR2, dNDVI, RdNDVI) using 4 different time windows from which to collate satellite imagery (16, 32, 48,  
 204 and 64 days). Following Cansler & McKenzie (2012) and Parks *et al.* (2014), we used interpolation to extract  
 205 remotely-sensed severity at the locations of the CBI field plots to better align remote and field measures  
 206 of severity. We extracted remotely-sensed severity values using both bilinear interpolation, which returns  
 207 a severity value weighted by the 9 pixel values nearest to the CBI plot location, and bicubic interpolation,  
 208 which returns a severity value weighted by the 16 pixel values nearest to the CBI plot location. In total, we

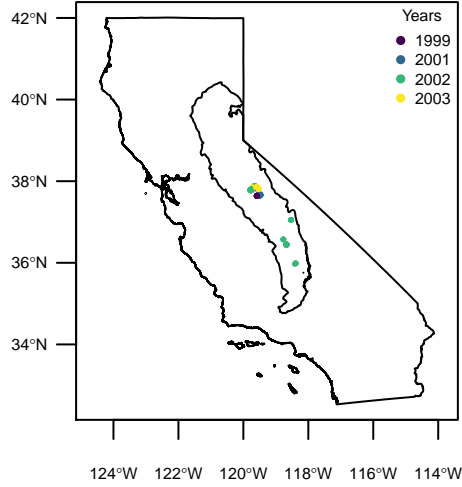


Figure 5: Location of CBI plots in the Sierra Nevada mountain range of California

fit 56 models (7 severity measures, 4 time windows, 2 interpolation methods) and performed five-fold cross validation using the `modelr` and `purrr` packages. To compare goodness of model fits with Miller & Thode (2007), Miller *et al.* (2009), and Parks *et al.* (2014), we report the average  $R^2$  value from the five folds for each of the 56 models but note that  $R^2$  for non-linear regressions do not have the same interpretation that they do for linear regression (i.e.,  $R^2$  can be greater than 1 for non-linear regression, so it can't be interpreted as the proportion of variation explained by the model). We used the Relative Burn Ratio (RBR) calculated using bicubic interpolation within a 48-day window as our response variable for analyses of vegetation heterogeneity, as it showed the best correspondence to field severity data measured as average  $R^2$  across the five folds.

## Remote sensing other conditions

### Heterogeneity of vegetation

We used texture analysis to calculate a remotely-sensed measure of forest heterogeneity (Haralick *et al.* 1973; Tuanmu & Jetz 2015). Within a moving square neighborhood window with sides of 90m, 150m, 210m, and 270m (corresponding to a moving neighborhood window of 0.81 ha, 2.25 ha, 4.41 ha, and 7.29 ha), we

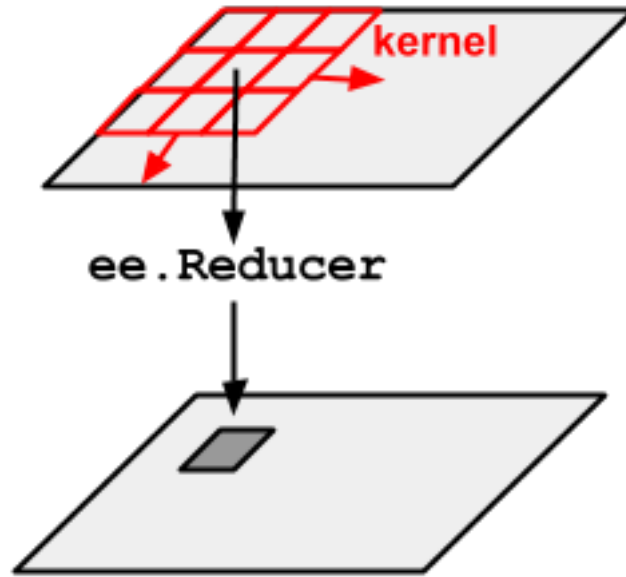


Figure 6: Neighborhood reducer that characterize each pixel as a summary of the neighboring pixels within a specified kernel. Image courtesy of Google and can be found at [https://developers.google.com/earth-engine/reducers\\_reduce\\_neighborhood](https://developers.google.com/earth-engine/reducers_reduce_neighborhood)

calculated heterogeneity for each focal pixel as the standard deviation of the NDVI values of its neighbors (not including itself).

#### Other vegetation conditions

We calculated pre-fire NDVI for each pixel.

We calculated the pre-fire mean NDVI in the same moving windows as the standard deviation of NDVI.

#### Topographic conditions

Elevation data were sourced from the Shuttle Radar Topography Mission (Farr *et al.* 2007), a 1-arc second digital elevation model. Slope and aspect were extracted from the digital elevation model. Per-pixel topographic roughness was calculated as the standard deviation of elevation values within a the same kernel sizes as those used for vegetation heterogeneity (approximately 90m, 150m, 210m, and 270m on a side and not including the central pixel). Some work has shown that terrain ruggedness (Holden *et al.* 2009), and particularly coarser-scale terrain ruggedness (Dillon *et al.* 2011), is an important predictor of wildfire severity.

We used the digital elevation model to calculate the potential annual heat load at each pixel, which is an

integrated measure of latitude, slope, and aspect (McCune & Keon (2002) with correction in McCune (2007)).  
 Folding the aspect about the northeast-southwest line, such that northeast becomes 0 radians and southwest  
 becomes  $\pi$  radians.

$$aspect_{folded} = |\pi - |aspect - \frac{5\pi}{4}|| \quad (9)$$

$$\begin{aligned} \log(PAHL) = & -1.467 + \\ & 1.582 * \cos(latitude) * \cos(slope) - \\ & 1.5 * \cos(aspect_{folded}) * \sin(slope) * \sin(latitude) - \\ & 0.262 * \sin(lat) * \sin(slope) + \\ & 0.607 * \sin(aspect_{folded}) * \sin(slope) \end{aligned} \quad (10)$$

Where PAHL is the potential annual heat load, folded\_aspect is determined by Eq. 9 and is in units of  
 radians, and both latitude and slope are extracted from a digital elevation model with units of radians.

## Fire weather conditions

The 100-hour fuel moisture data were sourced from the Gridmet product (Abatzoglou 2013) and were  
 calculated as the median 100-hour fuel moisture for the 3 days prior to the fire. We included a boolean  
 variable for extreme values of 100-hour fuel moisture if they were lower than 7.7%, since these values fall  
 below the 20<sup>th</sup> percentile of 100-hour fuel moisture for the Sierra Nevada region (Stephens *et al.* 2013).

## Modeling the effect of heterogeneity on severity

I scaled all predictor variables, and treated each individual fire as having a random intercept effect using the  
 following mixed effects model:

$$\begin{aligned} severity_{i,j} & \sim \mathcal{N}(\mu_{i,j}, \sigma_{error}) \\ \mu_{i,j} & = \beta_0 + \gamma_j + \beta_{heterogeneity} * heterogeneity\_i \end{aligned} \quad (11)$$

Each neighborhood size was substituted in turn for the heterogeneity of NDVI covariate, to generate a  
 candidate set of 4 models which were compared using AIC. The model with the best out-of-sample prediction

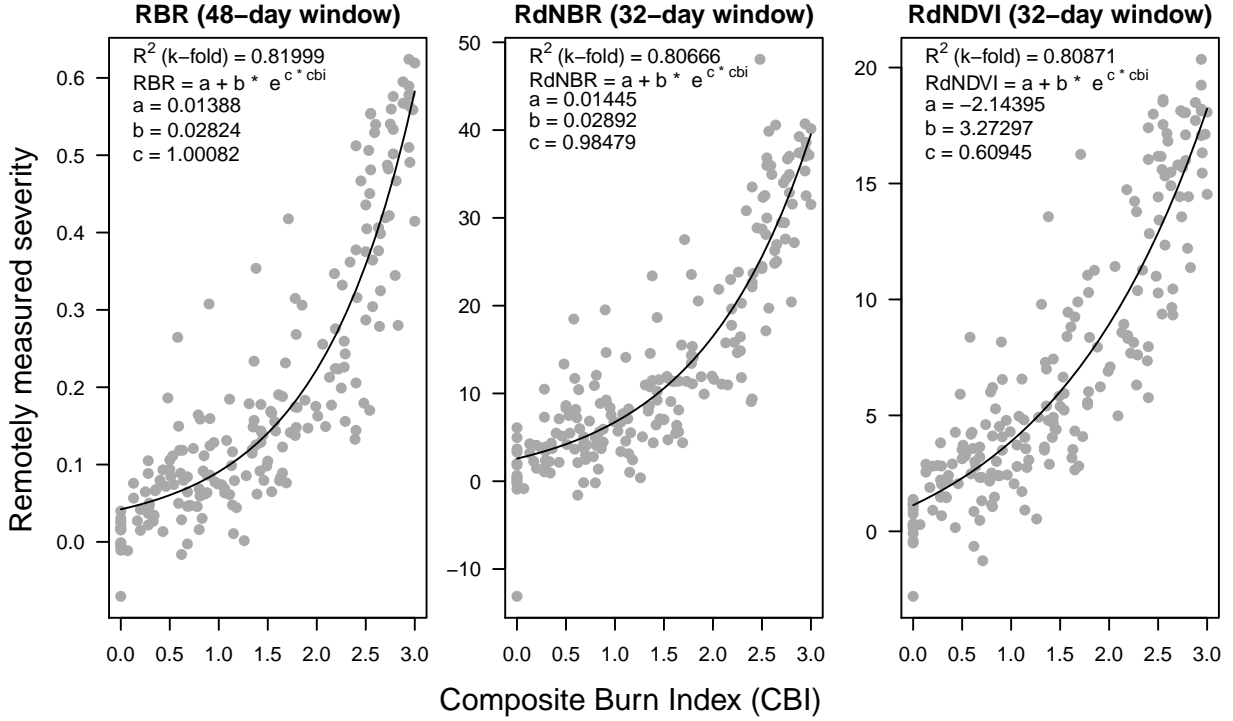


Figure 7: Calibration of three remotely-sensed severity metrics using new automated image collation algorithm to 208 field measures of severity.

was further analyzed by comparing the B coefficients to assess the relative effect of each predictor on wildfire severity.

## Statistical software and data availability

We used R for all statistical analyses (R Core Team 2017). We used the `lme4` package to fit mixed effects models (Bates *et al.* 2015).

Data are available via the Open Science Framework.

## Results

1. On-the-ground CBI measurements correlate well with our derived severity measurements. Our algorithm with its  $R^2$  puts it among the best (Edwards *et al.* 2018).
2. Heterogeneity of local NDVI is a meaningful measure of heterogeneity
3. The best model used heterogeneity at the smallest spatial scale.

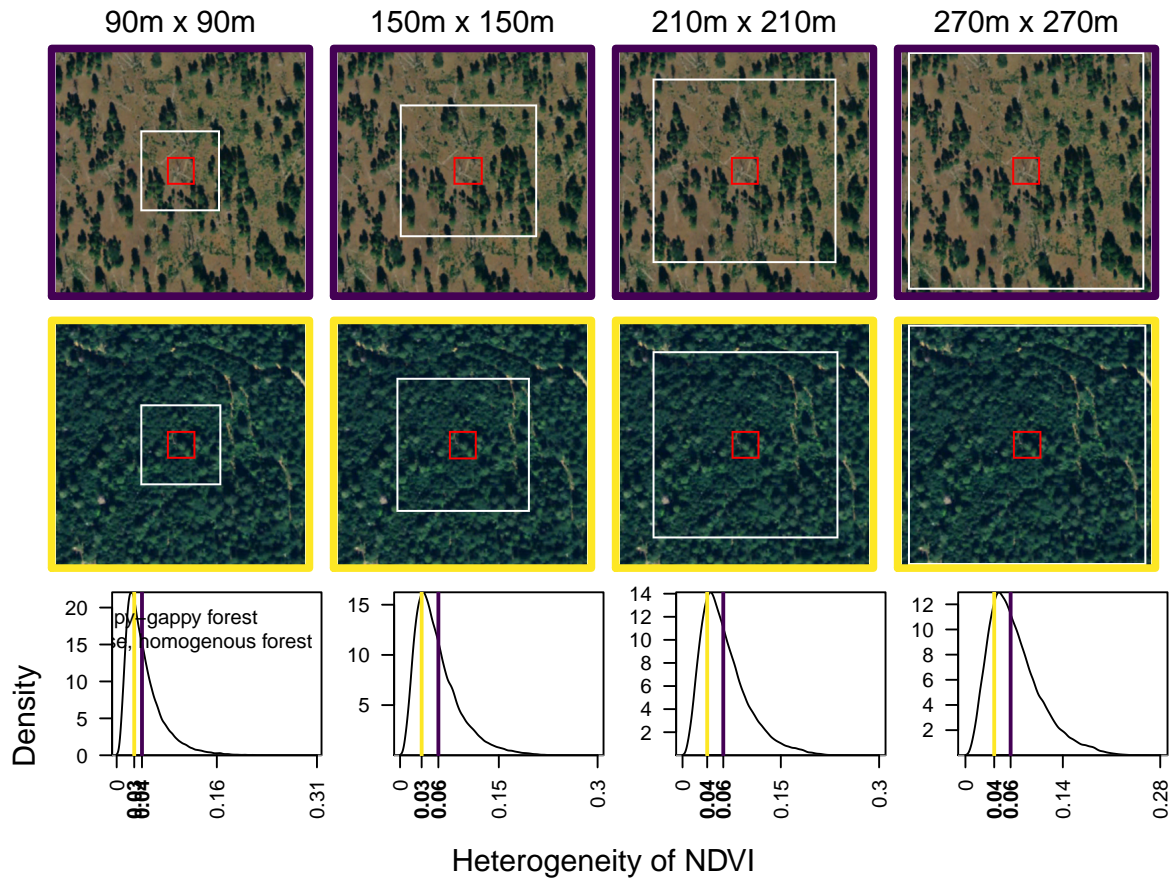


Figure 8: Highly heterogeneous forest in the Beaver Creek Pinery and homogenous forest nearby. Aerial photographs from USDA Farm Service Agency

4. Greater heterogeneity reduces wildfire severity.
5. The relative importance of heterogeneity depends on fire weather conditions (fuel moisture).

## Discussion

### Main points

1. We can programmatically measure severity with high accuracy and minimal user input– just a geometry and a fire alarm date.
2. We echo the conclusion of Zhu *et al.* (2006) that the validation of differences between pre- and postfire NDVI to field measured severity data, which uses near infrared reflectance, is comparable to validation using more commonly used severity metrics (e.g., RdNBR and dNBR) that rely on short wave infrared reflectance. One immediately operational implication of this is that the increasing availability of low-cost small unhumanned aerial systems (sUAS a.k.a. drones) and near infrared detecting imagers (e.g., those used for agriculture monitoring) may be used to measure wildfire severity at very high spatial resolutions.
3. We encourage people to make their on-the-ground severity data available with site location (including datum) and the alarm data for the fire the field data is measuring. Cloud-based GIS, central image hosting, and integration with powerful classification tools are ready right now to train on these data and advance our understanding of wildfire effects on the landscape.
- 4.

Our method should work best in denser vegetation such as forests, as the signal of a wildfire in other systems can be invisible in a matter of weeks (Goodwin & Collett 2014). This method would also require calibration with field data in other systems, as some severity metrics (such as RBR and RdNBR) have found limited success in other regions (Fernández-García *et al.* 2018).

The heterogeneity measure (standard deviation of NDVI in a 2ha moving window) can be fine-tuned and put into context by cross walking it with imagery at a finer spatial resolution (but with a cost in temporal resolution and time series depth; e.g. NAIP imagery at 1m resolution but with only 3 total images starting in 2008) (Dickinson *et al.* 2016). Additional metrics of heterogeneity such as vegetation patch size distributions or non-vegetated gap size distributions, may also be more tractable using the finer spatial resolution of NAIP imagery, though the specific fires used in these analyses will be limited to those taking place after 2008.



If heterogeneous forests are more resilient to fire, then we expect heterogeneity to be relatively maintained after fire.

The spatial autocorrelation inherent in analyses of spatial processes is an important consideration for model inference, because it challenges the assumptions of standard statistical techniques.

1.

Abatzoglou, J.T. (2013). Development of gridded surface meteorological data for ecological applications and modelling. *International Journal of Climatology*, 33, 121–131.

2.

Ackerly, D.D., Loarie, S.R., Cornwell, W.K., Weiss, S.B., Hamilton, H. & Branciforte, R. *et al.* (2010). The geography of climate change: Implications for conservation biogeography. *Diversity and Distributions*, 16, 476–487.

3.

Agashe, D. (2009). The stabilizing effect of intraspecific genetic variation on population dynamics in novel and ancestral habitats. *The American Naturalist*, 174, 255–67.

4.

Asner, G.P., Brodrick, P.G., Anderson, C.B., Vaughn, N., Knapp, D.E. & Martin, R.E. (2015). Progressive forest canopy water loss during the 2012–2015 California drought. *Proceedings of the National Academy of Sciences*, 2015, 201523397.

5.

Asner, G.P., Martin, R.E., Knapp, D.E., Tupayachi, R., Anderson, C.B. & Sinca, F. *et al.* (2017). Airborne laser-guided imaging spectroscopy to map forest trait diversity and guide conservation. *Science*, 355, 385–389.

6.

Baskett, M.L., Gaines, S.D. & Nisbet, R.M. (2009). Symbiont diversity may help coral reefs survive moderate climate change. *Ecological Applications*, 19, 3–17.

7.

Bastarrika, A., Chuvieco, E. & Martín, M.P. (2011). Mapping burned areas from landsat TM/ETM+ data with a two-phase algorithm: Balancing omission and commission errors. *Remote Sensing of Environment*, 115, 1003–1012.

8.

Bates, D., Maechler, M., Bolker, B. & Walker, S. (2015). *Fitting linear mixed-effects models using lme4*.

- 319 9.  
320 Boschetti, L., Roy, D.P., Justice, C.O. & Humber, M.L. (2015). MODIS-Landsat fusion for large area 30m  
321 burned area mapping. *Remote Sensing of Environment*, 161, 27–42.
- 322 10.  
323 Cadotte, M., Albert, C.H. & Walker, S.C. (2013). The ecology of differences: Assessing community assembly  
324 with trait and evolutionary distances. *Ecology Letters*, 16, 1234–1244.
- 325 11.  
326 Cansler, C.A. & McKenzie, D. (2012). How robust are burn severity indices when applied in a new region?  
327 Evaluation of alternate field-based and remote-sensing methods. *Remote Sensing*, 4, 456–483.
- 328 12.  
329 Chesson, P. (2000). Mechanisms of maintenance of species diversity. *Annual Review of Ecology and Systematics*,  
330 31, 343–366.
- 331 13.  
332 Clyatt, K.A., Crotteau, J.S., Schaedel, M.S., Wiggins, H.L., Kelley, H. & Churchill, D.J. *et al.* (2016).  
333 Historical spatial patterns and contemporary tree mortality in dry mixed-conifer forests. *Forest Ecology and*  
334 *Management*, 361, 23–37.
- 335 14.  
336 Collins, B.M., Lydersen, J.M., Everett, R.G., Fry, D.L. & Stephens, S.L. (2015). Novel characterization of  
337 landscape-level variability in historical vegetation structure. *Ecological Applications*, 25, 1167–1174.
- 338 15.  
339 Collins, B.M. & Stephens, S.L. (2010). Stand-replacing patches within a 'mixed severity' fire regime:  
340 Quantitative characterization using recent fires in a long-established natural fire area. *Landscape Ecology*, 25,  
341 927–939.
- 342 16.  
343 Connors, R.W., Trivedi, M.M. & Harlow, C.A. (1984). Segmentation of a high-resolution urban scene using  
344 texture operators. *Computer Vision, Graphics, and Image Processing*, 25, 273–310.
- 345 17.  
346 Crowther, T.W., Glick, H.B., Covey, K.R., Bettigole, C., Maynard, D.S. & Thomas, S.M. *et al.* (2015).  
347 Mapping tree density at a global scale. *Nature*, 525, 201–205.
- 348 18.

- 349 Culbert, P.D., Radeloff, V.C., St-Louis, V., Flather, C.H., Rittenhouse, C.D. & Albright, T.P. *et al.* (2012).  
350 Modeling broad-scale patterns of avian species richness across the Midwestern United States with measures  
351 of satellite image texture. *Remote Sensing of Environment*, 118, 140–150.
- 352 19.
- 353 De Frenne, P., Rodríguez-Sánchez, F., Coomes, D.A., Baeten, L., Verstraeten, G. & Vellend, M. *et al.* (2013).  
354 Microclimate moderates plant responses to macroclimate warming. *Proceedings of the National Academy of*  
355 *Sciences of the United States of America*, 110, 18561–5.
- 356 20.
- 357 De Santis, A., Asner, G.P., Vaughan, P.J. & Knapp, D.E. (2010). Mapping burn severity and burning  
358 efficiency in California using simulation models and Landsat imagery. *Remote Sensing of Environment*, 114,  
359 1535–1545.
- 360 21.
- 361 Dickinson, Y., Pelz, K., Giles, E. & Howie, J. (2016). Have we been successful? Monitoring horizontal forest  
362 complexity for forest restoration projects. *Restoration Ecology*, 24, 8–17.
- 363 22.
- 364 Dillon, G.K., Holden, Z.A., Morgan, P., Crimmins, M.A., Heyerdahl, E.K. & Luce, C.H. (2011). Both  
365 topography and climate affected forest and woodland burn severity in two regions of the western US, 1984 to  
366 2006. *Ecosphere*, 2, art130.
- 367 23.
- 368 Edwards, A.C., Russell-Smith, J. & Maier, S.W. (2018). A comparison and validation of satellite-derived fire  
369 severity mapping techniques in fire prone north Australian savannas: Extreme fires and tree stem mortality.  
370 *Remote Sensing of Environment*, 206, 287–299.
- 371 24.
- 372 Eidenshink, J., Schwind, B., Brewer, K., Zhu, Z.-l., Quayle, B. & Howard, S. (2007). A project for monitoring  
373 trends in burn severity. *Fire Ecology*, 3, 3–21.
- 374 25.
- 375 Farr, T., Rosen, P., Caro, E., Crippen, R., Duren, R. & Hensley, S. *et al.* (2007). The shuttle radar topography  
376 mission. *Reviews of Geophysics*, 45, 1–33.
- 377 26.
- 378 Fernández-García, V., Santamarta, M., Fernández-Manso, A., Quintano, C., Marcos, E. & Calvo, L. (2018).

379 Burn severity metrics in fire-prone pine ecosystems along a climatic gradient using Landsat imagery. *Remote*  
380 *Sensing of Environment*, 206, 205–217.

381 27.

382 Folke, C., Carpenter, S., Walker, B., Scheffer, M., Elmqvist, T. & Gunderson, L. *et al.* (2004). Regime shifts,  
383 resilience, and biodiversity in ecosystem management. *Annual Review of Ecology, Evolution, and Systematics*,  
384 35, 557–581.

385 28.

386 Ford, K.R., Ettinger, A.K., Lundquist, J.D., Raleigh, M.S. & Hille Ris Lambers, J. (2013). Spatial  
387 heterogeneity in ecologically important climate variables at coarse and fine scales in a high-snow mountain  
388 landscape. *PLoS ONE*, 8, e65008.

389 29.

390 Fry, D.L., Stephens, S.L., Collins, B.M., North, M.P., Franco-Vizcaíno, E. & Gill, S.J. (2014). Contrasting  
391 spatial patterns in active-fire and fire-suppressed Mediterranean climate old-growth mixed conifer forests.  
392 *PLoS ONE*, 9, e88985.

393 30.

394 Gao, B.C. (1996). NDWI - A normalized difference water index for remote sensing of vegetation liquid water  
395 from space. *Remote Sensing of Environment*, 58, 257–266.

396 31.

397 Gazol, A. & Camarero, J.J. (2016). Functional diversity enhances silver fir growth resilience to an extreme  
398 drought. *Journal of Ecology*.

399 32.

400 Goodwin, N.R. & Collett, L.J. (2014). Development of an automated method for mapping fire history captured  
401 in Landsat TM and ETM+ time series across Queensland, Australia. *Remote Sensing of Environment*, 148,  
402 206–221.

403 33.

404 Gorelick, N., Hancher, M., Dixon, M., Ilyushchenko, S., Thau, D. & Moore, R. (2017). Remote Sensing of  
405 Environment Google Earth Engine : Planetary-scale geospatial analysis for everyone. *Remote Sensing of*  
406 *Environment*, 202, 18–27.

407 34.

408 Graham, R.T., McCaffrey, S. & Jain, T.B. (2004). *Science basis for changing forest structure to modify*

409 *wildfire behavior and severity* ( No. April). US Department of Agriculture, Forest Service, Rocky Mountain  
410 Research Station, Fort Collins, CO.

411 35.

412 Gunderson, L.H. (2000). Ecological resilience– in theory and application. *Annual Review of Ecology and*  
413 *Systematics*, 31, 425–439.

414 36.

415 Hansen, M.C., Potapov, P.V., Moore, R., Hancher, M., Turubanova, S.A. & Tyukavina, A. (2013). High-  
416 resolution global maps of 21st-century forest cover change. *Science*, 342, 850–853.

417 37.

418 Haralick, R.M., Shanmugam, K. & Dinstein, I. (1973). Textural Features for Image Classification. *IEEE*  
419 *Transactions on Systems, Man, and Cybernetics*, SMC-3, 610–621.

420 38.

421 Hawbaker, T.J., Vanderhoof, M.K., Beal, Y.J., Takacs, J.D., Schmidt, G.L. & Falgout, J.T. *et al.* (2017).  
422 Mapping burned areas using dense time-series of Landsat data. *Remote Sensing of Environment*, 198, 504–522.

423 39.

424 Holden, Z.A., Morgan, P. & Evans, J.S. (2009). A predictive model of burn severity based on 20-year satellite-  
425 inferred burn severity data in a large southwestern US wilderness area. *Forest Ecology and Management*, 258,  
426 2399–2406.

427 40.

428 Holling, C.S. (1973). Resilience and Stability of Ecological Systems. *Annual Review of Ecology and Systematics*,  
429 4, 1–23.

430 41.

431 Huang, Q., Swatantran, A., Dubayah, R. & Goetz, S.J. (2014). The influence of vegetation height heterogeneity  
432 on forest and woodland bird species richness across the United States. *PLoS ONE*, 9.

433 42.

434 Keeley, J.E., Pausas, J.G., Rundel, P.W., Bond, W.J. & Bradstock, R.A. (2011). Fire as an evolutionary  
435 pressure shaping plant traits. *Trends in Plant Science*, 16, 406–11.

436 43.

437 Key, C.H. & Benson, N.C. (2006). Landscape assessment: Sampling and analysis methods. *USDA Forest*  
438 *Service General Technical Report RMRS-GTR-164-CD*, 1–55.

44.

Kolden, C.A., Smith, A.M.S. & Abatzoglou, J.T. (2015). Limitations and utilisation of Monitoring Trends in Burn Severity products for assessing wildfire severity in the USA. *International Journal of Wildland Fire*, 24, 1023–1028.

45.

Kotliar, N.B. & Wiens, J. a. (1990). Multiple Scales of Patchiness and Patch Structure: A Hierarchical Framework for the Study of Heterogeneity. *Oikos*, 59, 253–260.

46.

Larson, A.J. & Churchill, D. (2012). Tree spatial patterns in fire-frequent forests of western North America, including mechanisms of pattern formation and implications for designing fuel reduction and restoration treatments. *Forest Ecology and Management*, 267, 74–92.

47.

Lenoir, J., Graae, B.J., Aarrestad, P.A., Alsos, I.G., Armbruster, W.S. & Austrheim, G. *et al.* (2013). Local temperatures inferred from plant communities suggest strong spatial buffering of climate warming across Northern Europe. *Global Change Biology*, 19, 1470–1481.

48.

Lydersen, J.M., North, M.P., Knapp, E.E. & Collins, B.M. (2013). Quantifying spatial patterns of tree groups and gaps in mixed-conifer forests: Reference conditions and long-term changes following fire suppression and logging. *Forest Ecology and Management*, 304, 370–382.

49.

Mandle, L., Bufford, J.L., Schmidt, I.B. & Daehler, C.C. (2011). Woody exotic plant invasions and fire: Reciprocal impacts and consequences for native ecosystems. *Biological Invasions*, 13, 1815–1827.

50.

Masek, J.G., Vermote, E.F., Saleous, N.E., Wolfe, R., Hall, F.G. & Huemmrich, K.F. *et al.* (2006). A Landsat Surface Reflectance Dataset. *IEEE Geoscience and Remote Sensing Letters*, 3, 68–72.

51.

McCune, B. (2007). Improved estimates of incident radiation and heat load using non-parametric regression against topographic variables. *Journal of Vegetation Science*, 18, 751–754.

52.

McCune, B. & Keon, D. (2002). Equations for potential annual direct incident radiation and heat load.

469 *Journal of Vegetation Science*, 13, 603–606.

470 53.

471 Millar, C.I. & Stephenson, N.L. (2015). Temperate forest health in an era of emerging megadisturbance.  
 472 *Science*, 349, 823–826.

473 54.

474 Millar, C.I., Stephenson, N.L. & Stephens, S.L. (2007). Climate change and forests of the future: Managing  
 475 in the face of uncertainty. *Ecological Applications*, 17, 2145–2151.

476 55.

477 Miller, J.D., Knapp, E.E., Key, C.H., Skinner, C.N., Isbell, C.J. & Creasy, R.M. *et al.* (2009). Calibration and  
 478 validation of the relative differenced Normalized Burn Ratio (RdNBR) to three measures of fire severity in  
 479 the Sierra Nevada and Klamath Mountains, California, USA. *Remote Sensing of Environment*, 113, 645–656.

480 56.

481 Miller, J.D. & Thode, A.E. (2007). Quantifying burn severity in a heterogeneous landscape with a relative  
 482 version of the delta Normalized Burn Ratio (dNBR). *Remote Sensing of Environment*, 109, 66–80.

483 57.

484 Moritz, M.A., Morais, M.E., Summerell, L.A., Carlson, J.M. & Doyle, J. (2005). Wildfires, complexity, and  
 485 highly optimized tolerance. *Proceedings of the National Academy of Sciences*, 102, 17912–7.

486 58.

487 Näsi, R., Honkavaara, E., Lyytikäinen-Saarenmaa, P., Blomqvist, M., Litkey, P. & Hakala, T. *et al.* (2015).  
 488 Using UAV-based photogrammetry and hyperspectral imaging for mapping bark beetle damage at tree-level.  
 489 *Remote Sensing*, 7, 15467–15493.

490 59.

491 North, M.P., Stephens, S.L., Collins, B.M., Agee, J.K., Aplet, G. & Franklin, J.F. *et al.* (2015). Reform  
 492 forest fire management. *Science*, 349, 1280–1281.

493 60.

494 North, M., Stine, P., Hara, K.O., Zielinski, W. & Stephens, S. (2009). An Ecosystem Management Strategy  
 495 for Sierran Mixed- Conifer Forests. *General Technical Report PSW-GTR-220*, 1–49.

496 61.

497 Park Williams, A., Allen, C.D., Macalady, A.K., Griffin, D., Woodhouse, C.A. & Meko, D.M. *et al.* (2012).  
 498 Temperature as a potent driver of regional forest drought stress and tree mortality. *Nature Climate Change*,

3, 292–297.

62.

Parks, S.A., Dillon, G.K. & Miller, C. (2014). A new metric for quantifying burn severity: The relativized burn ratio. *Remote Sensing*, 6, 1827–1844.

63.

Prichard, S.J. & Kennedy, M.C. (2014). Fuel treatments and landform modify landscape patterns of burn severity in an extreme fire event. *Ecological Applications*, 24, 571–590.

64.

Questad, E.J. & Foster, B.L. (2008). Coexistence through spatio-temporal heterogeneity and species sorting in grassland plant communities. *Ecology Letters*, 11, 717–726.

65.

R Core Team. (2017). *R: A language and environment for statistical computing*. <http://www.r-project.org/>.  
R Foundation for Statistical Computing, Vienna, Austria.

66.

Raffa, K.F., Aukema, B., Bentz, B.J., Carroll, A., Erbilgin, N. & Herms, D.A. *et al.* (2009). A literal use of 'forest health' safeguards against misuse and misapplication. *Journal of Forestry*, 276–277.

67.

Raffa, K.F., Aukema, B.H., Bentz, B.J., Carroll, A.L., Hicke, J.A. & Turner, M.G. *et al.* (2008). Cross-scale drivers of natural disturbances prone to anthropogenic amplification: The dynamics of bark beetle eruptions. *BioScience*, 58, 501.

68.

Reusch, T.B.H., Ehlers, A., Hämmerli, A. & Worm, B. (2005). Ecosystem recovery after climatic extremes enhanced by genotypic diversity. *Proceedings of the National Academy of Sciences*, 102, 2826–2831.

69.

Rouse, J.W., Hass, R.H., Schell, J. & Deering, D. (1973). Monitoring vegetation systems in the great plains with ERTS. *Third Earth Resources Technology Satellite (ERTS) symposium*, 1, 309–317.

70.

Scheffer, M., Carpenter, S., Foley, J.A., Folke, C. & Walker, B. (2001). Catastrophic shifts in ecosystems. *Nature*, 413, 591–596.

71.



Scholl, A.E. & Taylor, A.H. (2010). Fire regimes, forest change, and self-organization in an old-growth mixed-conifer forest, Yosemite National Park, USA. *Ecological Applications*, 20, 362–380.

72.

Sikkink, P.G., Dillon, G.K., Keane, R.E., Morgan, P., Karau, E.C. & Holden, Z.A. *et al.* (2013). *Composite Burn Index (CBI) data and field photos collected for the FIRESEV project, western United States*. Forest Service Research Data Archive, Fort Collins, CO.

73.

Steel, Z.L., Safford, H.D. & Viers, J.H. (2015). The fire frequency-severity relationship and the legacy of fire suppression in California forests. *Ecosphere*, 6, 1–23.

74.

Stein, A., Gerstner, K. & Kreft, H. (2014). Environmental heterogeneity as a universal driver of species richness across taxa, biomes and spatial scales. *Ecology Letters*, 17, 866–880.

75.

Stephens, S.L. & Collins, B.M. (2004). Fire regimes of mixed conifer forests in the North-Central Sierra Nevada at multiple scales. *Northwest Science*, 78, 12–23.

76.

Stephens, S.L., Fry, D.L. & Franco-Vizcaíno, E. (2008). Wildfire and spatial patterns in forests in northwestern Mexico: The United States wishes it had similar fire problems. *Ecology and Society*.

77.

Stephens, S.L., Lydersen, J.M., Collins, B.M., Fry, D.L. & Meyer, M.D. (2015). Historical and current landscape-scale ponderosa pine and mixed conifer forest structure in the Southern Sierra Nevada. *Ecosphere*, 6, 1–63.

78.

Stephens, S.L., Moghaddas, J.J., Edminster, C., Fiedler, C.E., Haase, S. & Harrington, M. *et al.* (2013). Fire Treatment Effects on Vegetation Structure, Fuels, and Potential Fire Severity in Western U. S. Forests. *Ecological Applications*, 19, 305–320.

79.

Sugihara, N.G. & Barbour, M.G. (2006). Fire and California vegetation. In: *Fire in california's ecosystems* (eds. Sugihara, N.G., Van Wagtendonk, J.W., Shaffer, K.E., Fites-Kaufman, J. & Thode, A.E.). University of California Press, Berkeley; Los Angeles, CA, USA, pp. 1–9.

80.

Tilman, D. (1994). Competition and biodiversity in spatially structured habitats. *Ecology*, 75, 2–16.

81.

Trumbore, S., Brando, P. & Hartmann, H. (2015). Forest health and global change. *Science*, 349.

82.

Tuanmu, M.-N. & Jetz, W. (2015). A global, remote sensing-based characterization of terrestrial habitat heterogeneity for biodiversity and ecosystem modelling. *Global Ecology and Biogeography*, n/a–n/a.

83.

Turner, M.G., Donato, D.C. & Romme, W.H. (2013). Consequences of spatial heterogeneity for ecosystem services in changing forest landscapes: Priorities for future research. *Landscape Ecology*, 28, 1081–1097.

84.

USGS. (2017a). Product Guide: Landat 8 Surface Reflectance Code (LaSRC) Product. *USGS Professional Paper*, 4.2.

85.

USGS. (2017b). Product Guide: Landsat 4-7 Surface Reflectance (LEDAPS) Product. *USGS Professional Paper*, 8, 38.

86.

Veraverbeke, S. & Hook, S.J. (2013). Evaluating spectral indices and spectral mixture analysis for assessing fire severity, combustion completeness and carbon emissions. *International Journal of Wildland Fire*, 22, 707–720.

87.

Vermote, E., Justice, C., Claverie, M. & Franch, B. (2016). Preliminary analysis of the performance of the Landsat 8/OLI land surface reflectance product. *Remote Sensing of Environment*, 185, 46–56.

88.

Virah-Sawmy, M., Willis, K.J. & Gillson, L. (2009). Threshold response of Madagascar’s littoral forest to sea-level rise. *Global Ecology and Biogeography*, 18, 98–110.

89.

Walker, B., Holling, C.S., Carpenter, S.R. & Kinzig, A. (2004). Resilience, adaptability, and transformability in social-ecological systems. *Ecology and Society*, 9, 5.

90.

589 Westerling, A.L., Hidalgo, H.G., Cayan, D.R. & Swetnam, T.W. (2006). Warming and earlier spring increase  
590 western U.S. forest wildfire activity. *Science*, 313, 940–943.

591 91.

592 Wood, E.M., Pidgeon, A.M., Radeloff, V.C. & Keuler, N.S. (2012). Image texture as a remotely sensed  
593 measure of vegetation structure. *Remote Sensing of Environment*, 121, 516–526.

594 92.

595 Young, D.J.N., Stevens, J.T., Earles, J.M., Moore, J., Ellis, A. & Jirka, A.L. *et al.* (2017). Long-term climate  
596 and competition explain forest mortality patterns under extreme drought. *Ecology Letters*, 20, 78–86.

597 93.

598 Zhu, Z., Key, C., Ohlen, D. & Benson, N. (2006). Evaluate Sensitivities of Burn-Severity Mapping Algorithms  
599 for Different Ecosystems and Fire Histories in the United States. *Final Report to the Joint Fire Science*  
600 *Program, Project JFSP 01-1-4-12*, 1–35.